Cell Reports
Methods

Article

Investigation of synaptic connectivity in functional *in vitro* neuronal assemblies

Graphical abstract

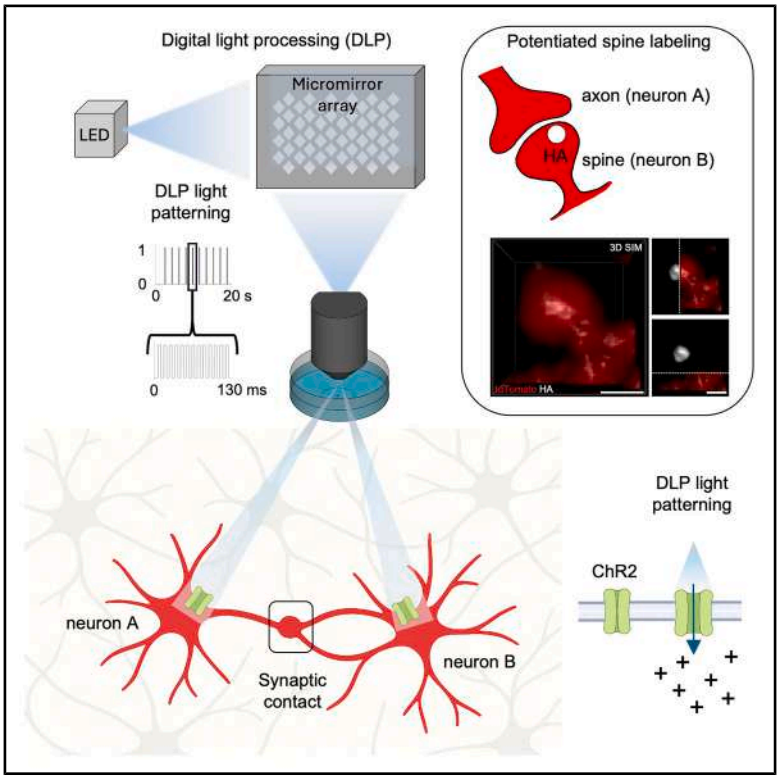

Highlights

- We develop an *in vitro* system to control activation of individual neurons in a network
- DLP-optogenetics system faithfully reproduces *in vivo* engram activation
- We demonstrate precise induction and tracking of synaptic strength
- This system enables reproducible, high-resolution functional connectivity studies

Authors

Clara Zaccaria, Asiye Malkoç, Ilya Auslender, Yasaman Heydari, Marco Canossa, Beatrice Vignoli, Lorenzo Pavesi

Correspondence

beatrice.vignoli@cnr.it

In brief

Zaccaria et al. describe a hybrid *in vitro* digital light processing (DLP)-optogenetics system to enable precise assembly and activation of neuronal pairs. This approach maps the emergence of functional synaptic connectivity with high spatiotemporal resolution, providing a modular platform to dissect the cellular and synaptic mechanisms underlying neuronal assemblies.

Zaccaria et al., 2026, Cell Reports Methods 6, 101265
January 26, 2026
https://doi.org/10.1016/j.crmeth.2025.101265

CellPress

Cell Reports Methods

CellPress
OPEN ACCESS

Article

Investigation of synaptic connectivity in functional *in vitro* neuronal assemblies

Clara Zaccaria,[1,4] Asiye Malkoç,[1,2,4] Ilya Auslender,[1] Yasaman Heydari,[1,3] Marco Canossa,[2,6] Beatrice Vignoli,[1,2,5,6,7,*] and Lorenzo Pavesi[1,6]

[1]Department of Physics, University of Trento, Povo 38123 TN, Italy
[2]Department of Cellular Computational and Integrative Biology (CIBIO), University of Trento, Povo 38123 TN, Italy
[3]Center for Mind/Brain Sciences (CIMeC), University of Trento, Rovereto 38068 TN, Italy
[4]These authors contributed equally
[5]Present address: Institute of Neuroscience, National Research Council of Italy, Padova section, 35121 Padova, Italy
[6]Senior author
[7]Lead contact
*Correspondence: beatrice.vignoli@cnr.it
https://doi.org/10.1016/j.crmeth.2025.101265

MOTIVATION Understanding how memory engrams, or neuronal ensembles, form and stabilize is a key question in neuroscience. While *in vivo* optogenetic approaches have demonstrated that reactivation of tagged engram neurons can trigger memory recall, the underlying micro-scale mechanisms remain elusive. The complexity of intact brain circuits limits the ability to monitor and manipulate individual synaptic connections during engram formation. Thus, simplified and controllable models are needed to dissect the fundamental principles by which coordinated neuronal activity gives rise to stable neuronal assemblies.

SUMMARY

Studies using genetic tagging and optogenetics demonstrated that reactivation of memory engrams, neuronal ensembles encoding specific learned information, can trigger memory recall and that synaptic potentiation among engram neurons is critical for memory persistence. However, the complexity of intact brain networks has limited mechanistic access to the processes underlying engram formation. Here, we introduce a hybrid *in vitro* platform that recapitulates, in a simplified and controllable setting, the core principles used *in vivo* to activate engrams. By combining digital light processing (DLP) with optogenetics, we imposed Hebbian co-activation of two targeted neurons, inducing the emergence of a functional cell assembly module. This artificial co-firing produced synaptic strengthening and spatial clustering of potentiated spines along the dendrites connecting the co-activated neurons, hallmarks of engram connectivity. Our system provides a reductionist yet biologically relevant framework to dissect, with high spatial and temporal resolution, the cellular and molecular determinants of cell assembly formation.

INTRODUCTION

One of the most significant advances in modern neuroscience is the experimental demonstration of memory engrams, specific neuronal ensembles that encode, store, and retrieve learned information.[1–5] Although the existence of engrams was postulated more than a century ago,[6–8] it is only in recent years that these memory traces have been directly identified and functionally manipulated *in vivo*. A pivotal contribution in this field came from the work of Tonegawa's group, which pioneered the use of activity-dependent genetic tagging combined with optogenetic stimulation to label and manipulate neurons activated during memory formation.[9] Their experimental strategy employed the TetTag system, in which the expression of channelrhodopsin-2 (ChR2) was driven by the immediate-early gene (IEG) promoter *c-Fos*. This method enabled selective tagging of neurons active during a specific behavioral episode, such as contextual fear conditioning, and their subsequent optogenetic reactivation in a neutral context. Remarkably, artificial reactivation of these neurons, in the absence of the original context, elicited a conditioned fear response, demonstrating that the reactivation of previously encoded engram cells is sufficient to trigger memory recall.[9] Further work investigated the synaptic basis of memory trace persistence. Hayashi-Takagi et al. (2015)[10] used a photoactivatable Rac1, targeted to potentiated synapses via Arc regulatory elements, to selectively label and eliminate spines formed during memory encoding. Light-induced activation of Rac1 led to spine loss and abolished memory recall, demonstrating that the

structural integrity of potentiated spines is essential for engram maintenance and reactivation.

Despite these breakthroughs, *in vivo* systems still limit our ability to resolve the internal structure of memory traces, as circuit complexity and restricted spatiotemporal access hinder high-resolution analysis of how synaptic potentiation shapes engram formation. To overcome these limitations, we developed a hybrid *in vitro* system that reproduces the experimental logic of *in vivo* engram tagging and activation, while enabling precise spatial and temporal assembly of individual neurons and synapses. This strategy was inspired by Donald O. Hebb's foundational postulate "When an axon of cell A is near enough to excite cell B and repeatedly or persistently takes part in firing it, some growth process or metabolic change takes place …"[6] In this simplified Hebbian framework, we experimentally engineered the activation of two paradigmatic neurons to mimic the conditions of coincident activity postulated by Hebb. Using a combination of digital light processing (DLP) and optogenetics, we induced synchronous firing and monitored the emergence of functional synaptic connectivity between the two neurons. This methodology preserves conceptual continuity with *in vivo* engram studies by applying the same experimental rationale. At the same time, it explicitly acknowledges the specific constraints of the *in vitro* context: the lack of a direct behavioral correlate confines interpretation to cellular and synaptic levels, while still providing mechanistic insights that are readily translatable to *in vivo* frameworks. Therefore, our *in vitro* platform is well-suited for modular cell assembly studies, providing a powerful experimental tool to investigate the cellular, synaptic, and molecular determinants of functional connectivity with high resolution and reproducibility.

RESULTS

The DLP-based system

We developed a DLP system (Figure 1A) combined with optogenetics to stimulate individual neurons within a network simultaneously. The detailed operational principle of the DLP-based system is illustrated in Figure S1. To assess the reliability of our system, we tested the optical resolution and optogenetic excitation on cortical embryonic cultures transduced with the adeno-associated virus AAV9-hSyn-hChR2(H134R)-EYFP (AAV-ChR2-YFP) (Table S1). This viral vector enabled selective ChR2 expression in most neurons within our cultures (Figure S2), allowing clear visualization of somata, dendritic arbors, and spines along dendritic shafts. However, fine axonal structures and presynaptic boutons could not be reliably resolved due to low contrast in thin processes and the diffraction-limited resolution of laser scanning confocal (LSC) microscopy, making bouton-to-spine assignment based solely on morphology unreliable. Nevertheless, light stimulation achieves varying scales of resolution, allowing for precise illumination of individual neuronal cell bodies or specific subregions of a neuron, down to single dendritic spines (Figure S1C). The cell density was calibrated to ensure sufficient network connectivity within the field of view (FOV), as demonstrated by immunocytochemical analysis using anti-SMI312 and anti-MAP2 antibodies, which target axons and dendrites, respectively (Figure S2).

Neurons were optically stimulated using a standard patterned illumination protocol (Figure 1B) known to induce long-term potentiation (LTP).[11] Confirmation comes from experiments that combined DLP illumination of a selected group of neurons within a network and LTP recording using a multi-electrode array (MEA). We observed that patterned light stimulation successfully induced LTP in certain areas of connectivity within the neuronal network (Figures 1C and 1D).

Generation of prototypical cell assembly modules

Our primary goal was to generate discrete modules of light-activated neurons, serving as prototypical examples of Hebb's "cell assemblies."[6] Using patterned light on neurons A and B simultaneously, we generate modules of two activated neurons (Figure 2A). Initially, we assess neuron responsiveness by imaging Ca^{2+} fluctuation before, during, and after the light stimulation using the Ca^{2+} indicator X-Rhod-1 (Figure 2B). We show that most neurons of the two-neuron modules responded to optical stimulation with a significant increase in X-Rhod-1 fluorescence intensity ($\Delta F/F$) compared to nearby non-illuminated neurons within the FOV (Figure 2C). When light stimulation was applied to individual neurons, we observed a similar increase in $\Delta F/F$ levels (Figure S3). Although the stimulated neurons are not isolated in their activity, these results indicate that our stimulation protocol can reliably and specifically activate one or two neurons without substantially recruiting the surrounding network. Moreover, neurons with ChR2-YFP fluorescence intensity (FI) exceeding 200 a.u. consistently displayed robust Ca^{2+} responses upon stimulation (Figures 2C and S3C), indicating that variations in ChR2-YFP above this treshold did not compromise the accuracy of our Ca^{2+} measurements.

Next, we examined whether light stimulation induces changes in the expression of cFos. This IEG marks active neurons, and its promoters enable selective recruitment of engram cells in behavioral experiments.[3,12] Ninety minutes after stimulation, cFos expression was elevated in neurons exposed to the light stimulus compared to non-illuminated neurons within the FOV or outside (Figure 2D).

In summary, we integrated optical stimulation, optogenetics, electrophysiology, Ca^{2+} imaging, and marker-based activity assessments to activate prototypical two-neuron modules within a neural network.

Spatial-temporal analysis of synaptic strengthening

To validate the functional assembly of neurons A and B in our experimental setup and to empirically support Hebb's postulate, we investigated whether patterned light stimulation could induce synaptic strengthening between the illuminated neurons. We integrated our system with SynActive (SA) technology, a genetically engineered platform that utilizes regulatory elements from Arc mRNA in combination with synapse-targeting peptides.[11] Using an inducible Tet-On system for controlled expression, this approach enables the expression of tags, such as Venus and hemagglutinin (HA-tag), specifically at potentiated spines (Table S1). Neurons were initially transfected with constructs (1) TreP-Arc3′-Nend-PSDTag-Venus-HA-Arc5′UTR; (2) CAG-rtTA-IRES-TdTomato, collectively referred to as SA-tdTomato; and (3) pAAV.CAG.hChR2

CellPress
OPEN ACCESS

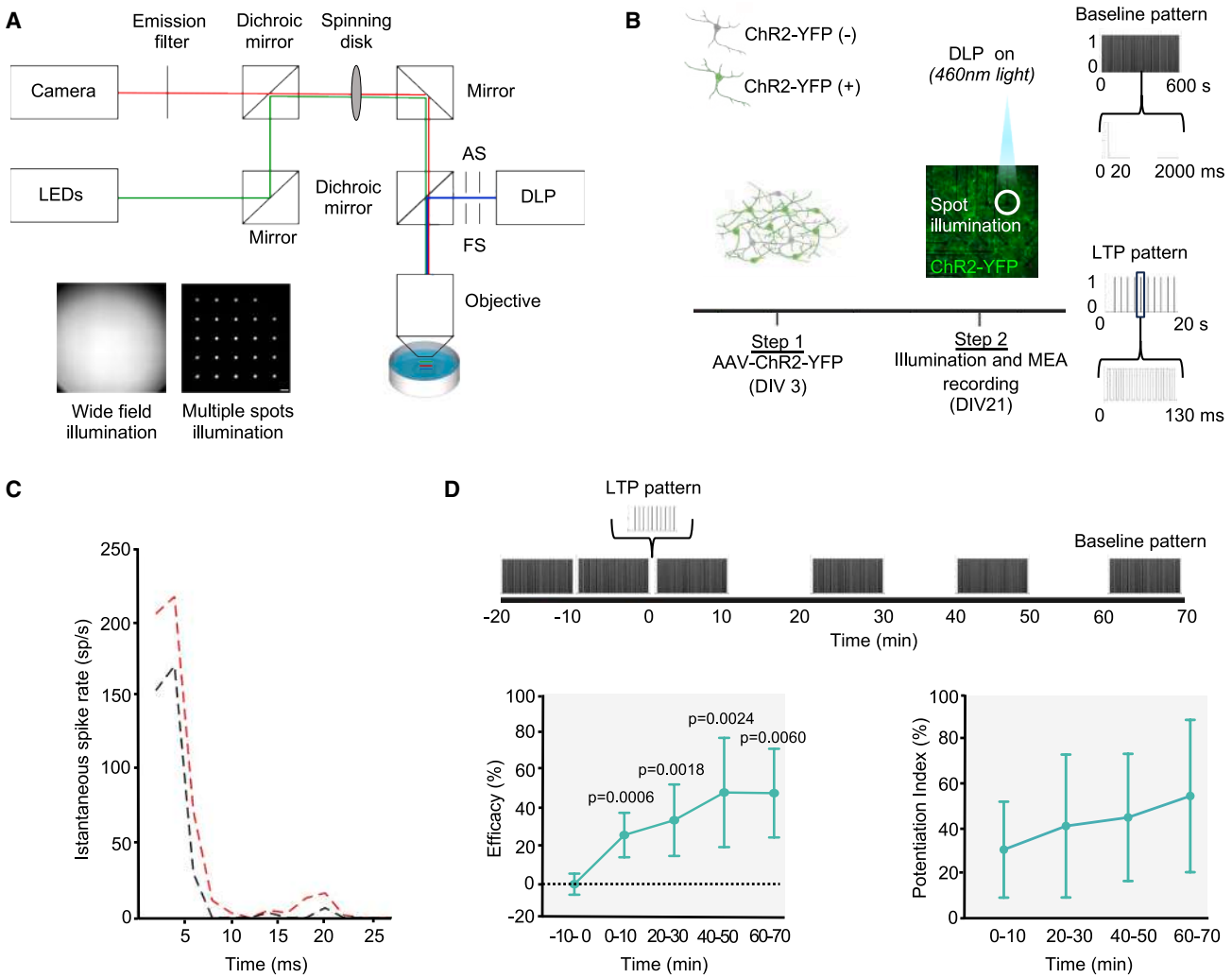

Figure 1. SD setup, implemented with DLP and MEA recording

(A) Scheme of the SD setup implemented with DLP. AS and FS refer to the aperture stop and the field stop diaphragms, respectively. Representative light patterns for wide-field and multiple spot illumination are shown.

(B) Schematic diagram of the experimental procedures and the temporal patterns used for baseline (20 ms light pulses at a frequency of 0.5 Hz for a duration of 10 min) and LTP light stimulation (10 sets of 13 light pulses delivered at a frequency of 100 Hz, duty cycle 50%, with a repetition frequency of 0.5 Hz).

(C) Representative post-stimulus time histogram recorded from a single electrode in one experiment before (black) and 20 min after (red) the LTP stimulation. Bin size = 2 ms.

(D) Upper: timeline representation of the MEA experimental protocol. Lower: efficacy (average response efficacy across electrodes at different time point) and potentiation index (quantification of the percentage of electrodes exceeding the 20% efficacy threshold) measured at different time points after the LTP-inducing light stimulation. Data are mean ± SD (n = 6 experiments; unpaired t test).

(H134R)-mCherry.WPRE.SV40 (ChR2-mCherry) (Table S1). Although mCherry and tdTomato fluorescence signals are spectrally indistinguishable, this does not pose a limitation, as the high co-transfection efficiency ensures that all constructs are expressed within the same neuronal population. Live imaging experiments using spinning disk (SD) microscopy show dendritic spines of transfected neurons A and B before illumination (Figure 3B). Spines that initially lack Venus fluorescence progressively accumulate the fluorescent signal 60 and 90 min after optical stimulation, indicating synaptic strengthening. We also observed spines that emerged exclusively after illumination and exhibited robust Venus fluorescence 90 min later (Figure 3C). Overall, our finding indicates that both pre-existing and newly formed spines are strengthened in direct response to optical stimulation.

Quantitative analysis was performed by detecting HA-tag immunofluorescence in neurons transfected with SA-tdTomato and transduced with AAV-ChR2-YFP 90 min after illumination (Figure 4A). The HA-tag signal was analyzed using LSC microscopy (Figures 4C and S4) as well as structured illumination microscopy (SIM) (Figure 4D).[13–15] Illuminated neurons A and B exhibited a significant increase in HA-tag+ spines

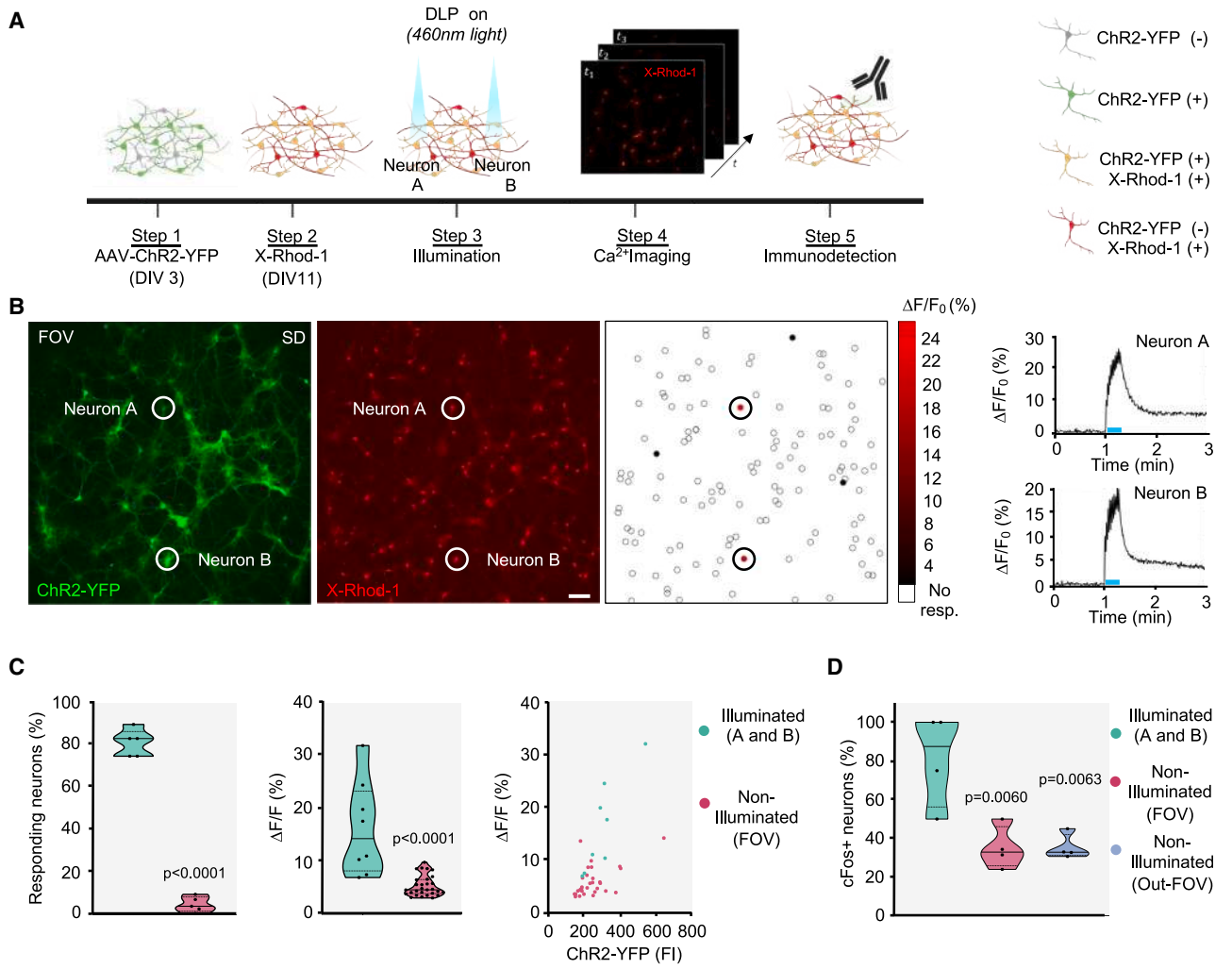

Figure 2. The prototypical cell assembly module

(A) Schematic diagram of the experimental procedures.

(B) SD images depicting ChR2-YFP (average transduction efficiency: 75% ± 3%) and X-Rhod-1 fluorescence signals in a representative neuronal network. Scale bar, 50 μm. Illuminated neurons (A and B) are highlighted (circles). A heatmap illustrates the percentage change in fluorescence (ΔF/F) calculated in automatically detected ROIs. The diagrams display fluorescence changes (ΔF/F) recorded from the soma of neurons A and B, before, during, and after light stimulation (blue line).

(C) Left: quantification of the number of responding neurons A and B and non-illuminated neurons in the FOV (n = 5 experiments; unpaired t test). Middle: quantification of ΔF/F (n = 8 cells for illuminated (A and B); n = 29 cells for non-illuminated [FOV]; Mann-Whitney test). Right: ΔF/F plotted against the ChR2-YFP FI (n = 8 cells for illuminated [A and B]; n = 31 cells for non-illuminated [FOV]). Violin plots depict median (continuous line) and quartiles (dashed line).

(D) Percentage of A and B neurons, non-illuminated neurons within the FOV and Out-FOV expressing cFos (n = 4 experiments; illuminated [A and B]: cFos+ neurons = 16, total counted neurons = 20; FOV: cFos+neurons = 190, total counted neurons = 501; outFOV: cFos+neurons = 240, total counted neurons = 779; one-way ANOVA test). Violin plots depict median (continuous line) and quartiles (dashed line).

along their dendritic branches compared to non-stimulated neurons within and outside the FOV (Figure 4B). In contrast, neurons that were illuminated individually showed no similar increase in HA-tag+ spine (Figures 4E and 4F), confirming that postsynaptic activation alone is not sufficient to induce synaptic potentiation. This supports the principle that both presynaptic input and postsynaptic depolarization are essential for strengthening dendritic spines, highlighting the need for coordinated activity between stimulated neurons within the network.

To validate this conclusion, we conducted experiments using light stimulation in the presence of tetrodotoxin (TTX), which specifically blocks voltage-gated sodium channels and prevents action potentials in neurons, while leaving ChR2 activity unaffected.[16] The previously observed increase in HA-tag+ spines of light-stimulated neurons A and B was abolished by TTX (Figure 4B), reinforcing the idea that synaptic strengthening occurs when target neurons receive pre- and post-synaptic inputs.

Additional control procedures related to our experimental methods are reported in Figure S5.

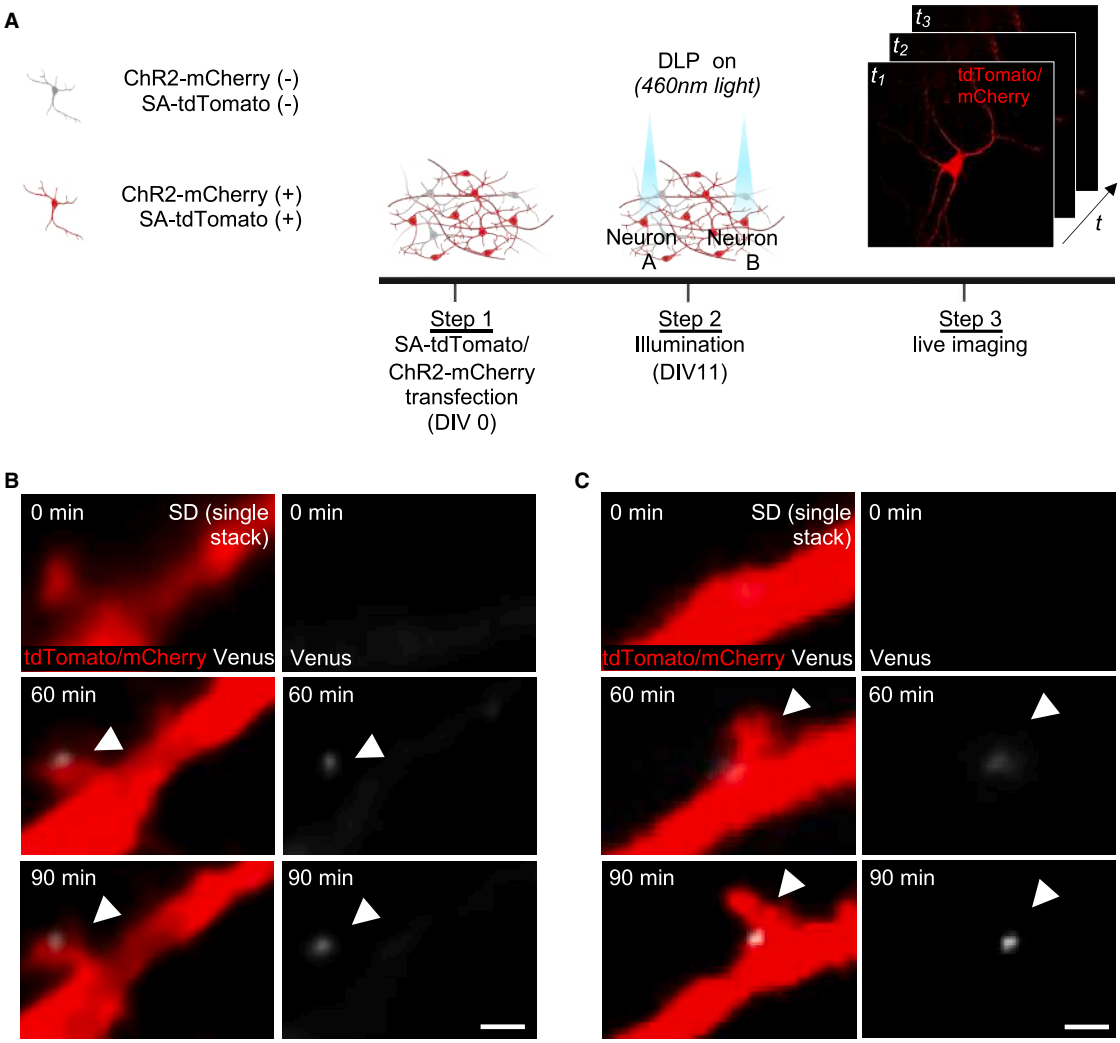

Figure 3. Tracking Venus tag accumulation in spine using live imaging

(A) Schematic diagram of the experimental procedures (sample size is n = 5 FOV/culture well).

(B) Dendritic spines expressing tdTomato gradually accumulate the Venus tag signal 60 and 90 min after the light stimulus. Arrowhead indicates HA-tag+ spine. Scale bar, 1 μm.

(C) Dendritic spines expressing tdTomato appeared and exhibited Venus tag fluorescence 60 and 90 min after illumination. Arrowhead indicates HA-tag+ spine. Scale bar, 1 μm.

Patterned distribution of potentiated synapses

Recent studies have demonstrated that synaptic potentiation is not uniformly distributed across dendritic structures; instead, it exhibits spatial specificity, with co-activated neurons showing enhanced synaptic strength at dendritic locations. This spatially biased potentiation is thought to be a critical mechanism underlying the formation of functional neuronal ensembles shaping the wiring of neural circuits.[17–23] We, therefore, investigated whether optical stimulation of the two-neuron modules can direct synaptic strengthening toward a specific pattern. To address this issue, we evaluated the spatial distribution of HA-tag+ spines in illuminated neurons, analyzing their relative positioning within dendritic processes. We defined the orientation between neurons A and B as 0° and evaluated the orientation of each dendritic process relative to this reference angle (Figure 5A). Dendrites showing an angle range of 0°–90° and 270°–360° were classified as IN-dendrites, while dendrites oriented in the opposite direction (angle range 90°–180° and 180°–270°) were classified as OUT-dendrites (Figure 5A). We then plotted the HA-tag+ spines in each dendrite according to their IN-or-OUT categorization. Our data show a preferential distribution of HA-tag+ spines toward IN-dendrites (Figures 5B and 5C). This polarized distribution was absent when neurons were illuminated with a weaker stimulation protocol (Figure 5C), which failed to induce synaptic potentiation (Figure S5B), or when exposed to TTX (Figure 5C). This suggests that the preferred orientation of HA-tag+ spines is linked to the synchronized, reciprocal activity triggered by optical stimulation, and, thus, shapes their wiring. To support

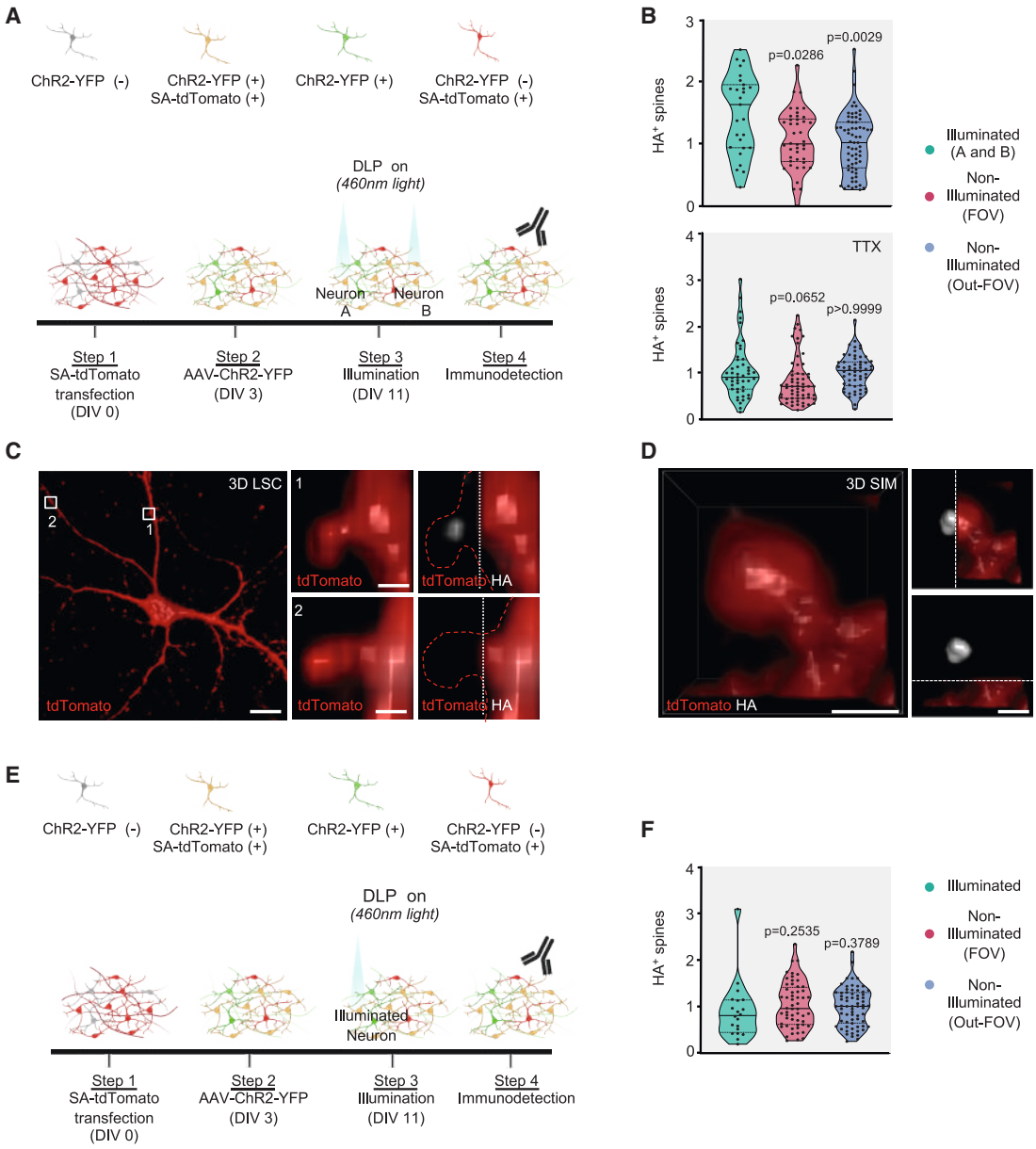

Figure 4. Quantitative analysis of HA-tag accumulation in spines

(A) Experimental procedures for two-neuron illumination.

(B) Upper: quantification of HA-tag+ spines (%) in illuminated neurons A and B and non-illuminated neurons in the FOV and Out-FOV (n = 27 dendrites for illuminated [A and B]; n = 42 dendrites for non-illuminated [FOV]; n = 67 dendrites for non-illuminated [Out-FOV]; Kruskal-Wallis test). Lower: violin plot as in upper panel in the presence of TTX (n = 40 dendrites for illuminated [A and B]; n = 61 dendrites for non-illuminated [FOV]; n = 58 dendrites for non-illuminated [Out-FOV]; Kruskal-Wallis test). Data are normalized over the Out-FOV. Violin plots depict median (continuous line) and quartiles (dashed line).

(C) Left: 3D LSC images of a stimulated neuron expressing tdTomato. Scale bar: 10 μm. Right: the magnification of HA-tag+ (1) and HA-tag− (2) spines is shown; tdTomato signal was partially removed to unmask the HA signal. Scale bars, 1 μm.

(D) Left: 3D SIM images of an HA-tag+ spine. Right: the same spine is shown with the tdTomato signal partially (upper) or fully (lower) removed. Scale bars, 1 μm.

(E) Experimental procedures for single-neuron illumination.

(F) Quantification of HA-tag+ spines (%) in single illuminated neurons and non-illuminated neurons within the FOV and Out-FOV (n = 27 dendrites for illuminated; n = 42 dendrites for non-illuminated [FOV]; n = 67 dendrites for non-illuminated [Out-FOV]; Kruskal-Wallis test).

Data are normalized over the Out-FOV. Violin plots depict median (continuous line) and quartiles (dashed line).

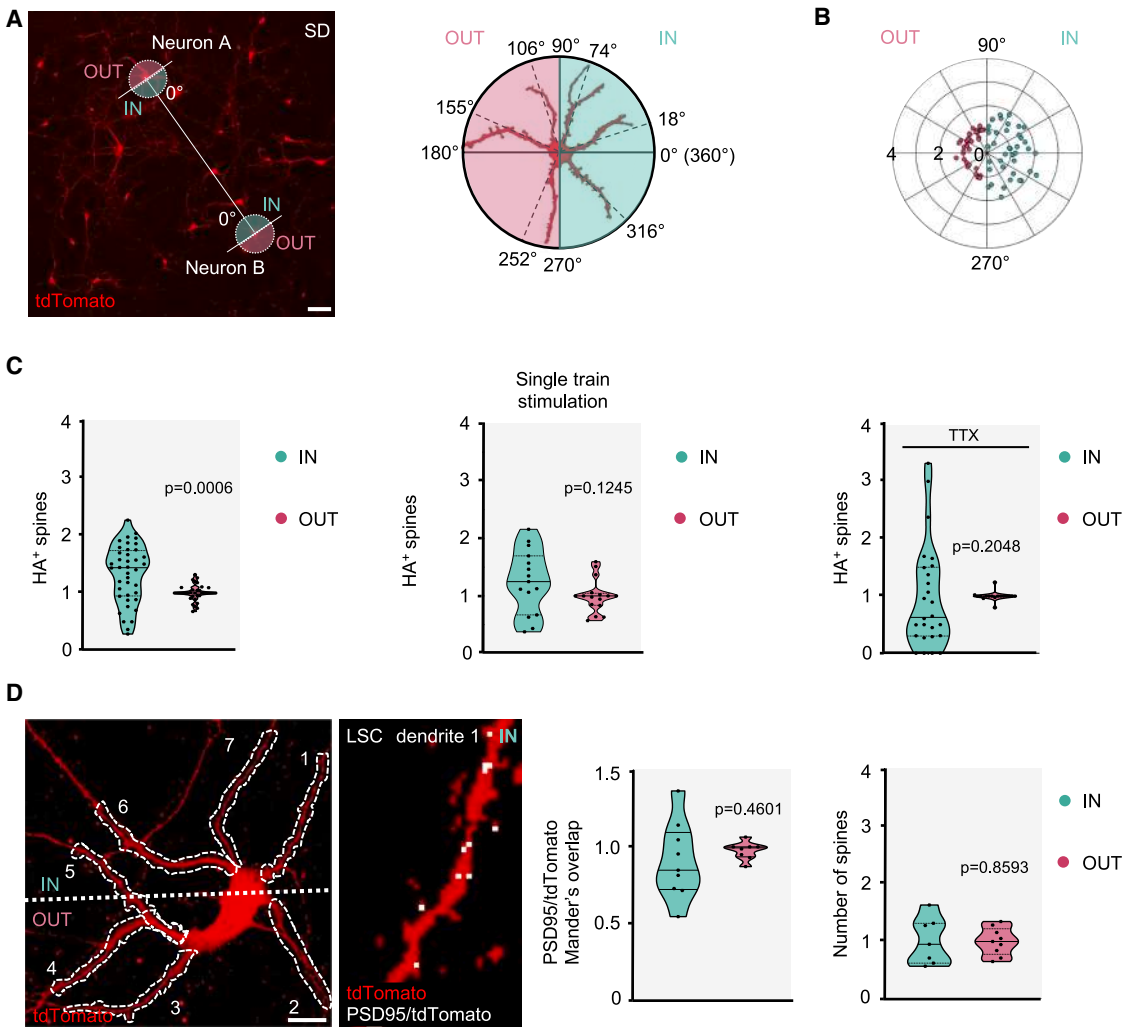

Figure 5. Spine distribution in light-stimulated neurons

(A) Left: SD image of tdTomato-expressing neurons within a network (average transfection efficiency: 35% ± 4%). The reference orientation between neurons A and B is marked as 0° on the polar plots. Dendrites falling within an angle range of 0°–90° and 270°–360° were classified as IN-dendrites (green), while dendrites within an angle range 90°–180° and 180°–270° are classified as OUT-dendrites (pink). Right: schematic representation of the polar plot displaying dendrites according to their oriented angles. Scale bar, 50 μm.

(B) Polar plot illustrates the distribution of HA-tag+ spines along the IN/OUT dendrites.

(C) Left: HA-tag+ spines quantification (%) of IN/OUT dendrites (n = 40 dendrites IN; n = 37 dendrites OUT; Mann-Whitney test). Middle: HA-tag+ spines quantification (%) of IN/OUT dendrites in neurons stimulated with 1 train stimulation (n = 9 dendrites IN; n = 8 dendrites OUT; Unpaired t test). Right: HA-tag+ spines quantification (%) of IN/OUT dendrites in the presence of TTX (n = 25 dendrites IN; n = 37 dendrites OUT; Mann-Whitney test). Data are normalized to the average of the "OUT" dendrites. Violin plots depict median (continuous line) and quartiles (dashed line).

(D) Left: LSC image of a tdTomato-expressing neuron in which dendrites 1–7 (white dashed) are indicated. Two-time magnification of dendrite 1 showing PSD95/tdTomato co-localization. Middle: quantification of PSD95/tdTomato colocalization in IN/OUT processes using Mander's overlap coefficient. (n = 9 dendrites for IN; n = 8 dendrites for OUT; unpaired t test). Right: morphological quantification of spines in IN/OUT dendrites (n = 7 dendrites for IN; n = 9 dendrites for OUT; unpaired t test). Data are normalized to the average of the "OUT" dendrites. Scale bar, 10 μm. Violin plots depict median (continuous line) and quartiles (dashed line).

this conclusion, we demonstrated that the overall distribution of post-synaptic sites, evaluated by both morphological assessment and PSD95/tdTomato colocalization, did not significantly change between the dendrites of illuminated neurons (Figure 5D), suggesting that the observed changes in HA-tag+ spines involve functional rather than anatomical reorganization.

Direct targeting of synaptic ensembles

Our system allows precise scaling of DLP illumination to dendritic spine resolution (Figure S1C). Using this approach, we specifically illuminated spines on target dendrites (Figure 6A). This methodology allows the direct strengthening of synaptic contacts, while minimizing overall neuronal stimulation.

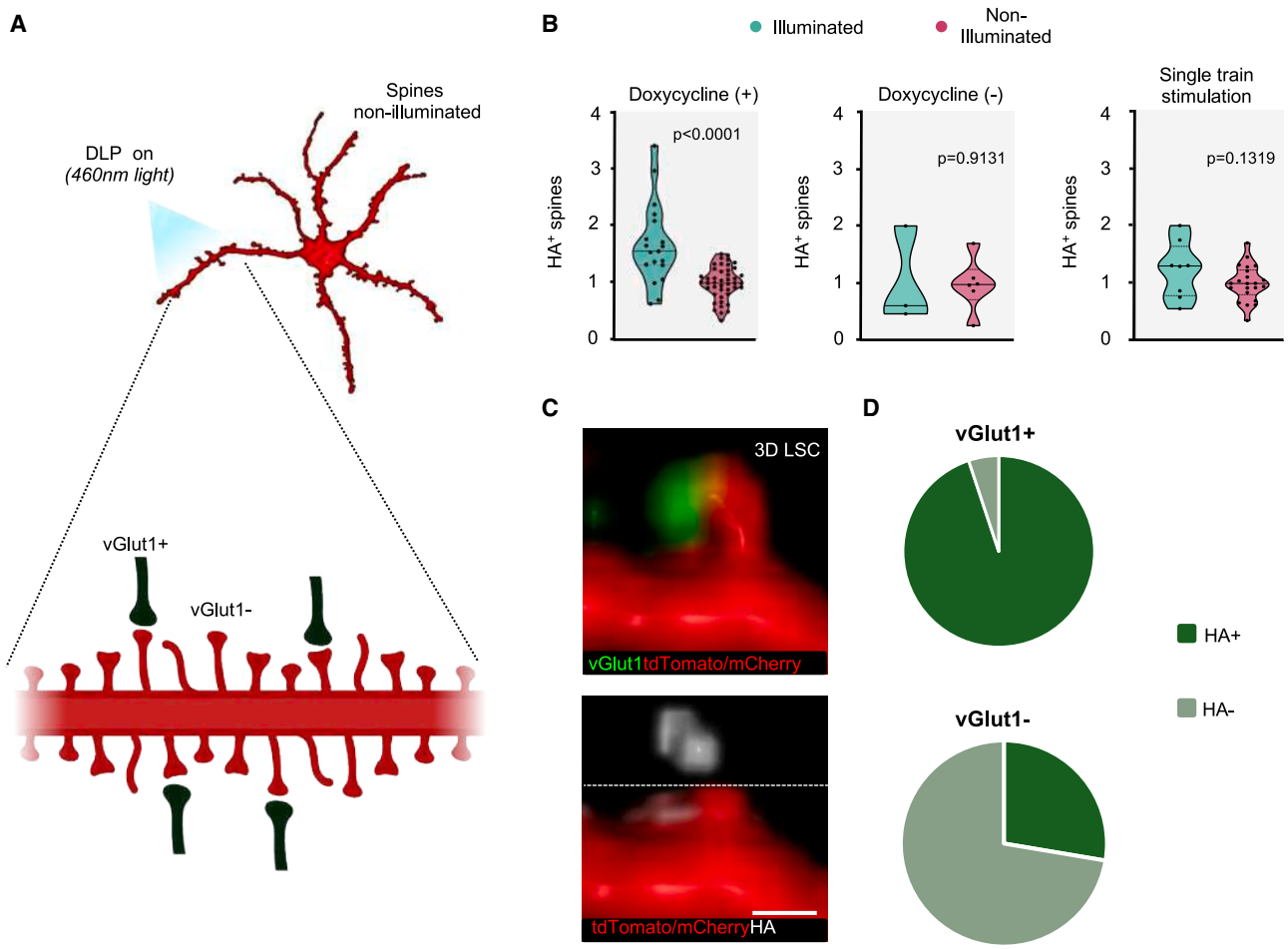

Figure 6. Induction of targeted synaptic strengthening

(A) Local optical stimulation of a dendritic segment, highlighting postsynaptic structures that are either connected to presynaptic terminals (vGlut+) or not (vGlut−).

(B) Left: quantification of HA+ spines (%) of illuminated dendrites in the presence (n = 19 dendrites for illuminated; n = 44 dendrites for non-illuminated dendrites; unpaired t test) and absence (n = 3 dendrites for illuminated; n = 3 dendrites for non-illuminated dendrites; unpaired t test) of doxycycline. Right: quantification of HA-tag+ spines (%) of dendrites illuminated with single-train stimulation and non-illuminated dendrites (n = 8 dendrites for 1 single-light stimulation; n = 22 dendrites for non-illuminated dendrites, unpaired t test). Data are normalized to the average of non-illuminated dendrites for each neuron. Violin plots depict median (continuous line) and quartiles (dashed line).

(C) Top: 3D LSC images of a spine expressing tdTomato/mCherry, positioned opposite to the vGlut1 signal. Bottom: the same spine with the HA-tag signal unmasked. Scale bars, 1 μm.

(D) Pie charts illustrate the percentage of HA-tag+ and HA-tag− spines. The upper panel represents spines positioned opposite Vglut1+ afferents, while the lower panel shows spines lacking Vglut1 expression.

Using a 60X water immersion objective, we locally illuminate a portion of a dendrite in neurons expressing SA-tdTomato and ChR2-mCherry (Figure 6A). Following illumination, we observed a significant increase in HA-tag+ spines in the illuminated regions after a latency of 90 min, compared to similar portions in the non-illuminated dendrites of the same neuron. To assess whether potentiated spines required coincident pre- and postsynaptic activation, we focused on illuminated dendritic segments and compared HA-tag+ versus HA-tag− spines in relation to the presynaptic marker vGLUT1, noting that presynaptic boutons could not be directly visualized. We reasoned that a potentiated spine must have a presynaptic contact, ruling out the possibility that potentiation arises from postsynaptic depolarization alone, as supported by our dual-versus single-neuron illumination experiments (Figures 3 and 4). We observed a high correspondence between HA-tag+ spines and opposite vGLUT1 puncta (Figures 6C and 6D). In contrast, most spines lacking presynaptic input on the same dendrite (vGLUT1−) remained non-potentiated (Figure 6D). The increase in HA-tag+ spines was absent when doxycycline was omitted or when a weaker stimulation protocol was applied (Figures 6B, S5B, and S5C), suggesting that potentiation occurred at bona fide excitatory synapses and was not merely driven by ChR2-mediated postsynaptic depolarization.

Overall, this experimental approach establishes a highly controlled environment for inducing synaptic strengthening in defined neuronal ensembles, allowing for precise manipulation and observation of the functional assembly and connectivity within neural networks. By targeting specific spines or clusters, we can systematically explore how various patterns of activity affect network assembly and the overall wiring of circuits.

DISCUSSION

Our hybrid DLP system is a reliable tool for investigating the principles of synaptic ensemble strengthening in small-scale neuronal assemblies. It enables precise tracking and induction of artificial synaptic strengthening by integrating cutting-edge techniques such as optogenetics and synaptic imaging. This methodology is deeply anchored in Hebb's foundational postulate, offering a solid theoretical framework that guides our research approach. At the core of our investigation is the reinforcement of synaptic strength between what we have termed "Hebbian" neurons A and B. This critical process is essential for creating functional connectivity supporting the formation of neuronal assemblies within the brain.[24,25] The inherent simplicity of the two-neuron module, used as a building block for more complex circuits, offers an opportunity to explore the basic principles of functional circuits in situations where *in vivo* studies are not feasible.

Observational studies have indicated that changes in IEG expression triggered by learning are closely associated with engram encoding and can predict future retrieval activities.[12] Common markers for identifying engram cells in living organisms include increased intracellular Ca^{2+} levels and the expression of cFos and Arc. Although these markers cannot define an engram *in vitro*—since an engram is identified through memory assessment *in vivo*—their presence in our system supports the identification of functional neuron ensembles that exhibit key characteristics of neuron assembly. Likewise, the observed potentiation of spines between illuminated neurons A and B, as demonstrated through SA labeling, strongly validates our methodological approach. These findings not only confirm the system's effectiveness in inducing, detecting, and quantifying synaptic changes between active neurons but also underscore its reliability in studying their spatial organization in synaptic ensembles.

The architectural organization of active synapses within functional circuits is critical for understanding their wiring. Our study highlights that the specific orientations in which synaptic connections are strengthened play a crucial role in locating regions of heightened activity. Neurons subjected to patterned illumination formed connections that were not only strengthened but also directionally organized. This suggests an adaptive network mechanism that improves information processing efficiency and emphasizes how synchronized neural activity contributes to cell assembly formation by potentially integrating neurons across different brain areas more effectively. Our methodology, applying the same experimental rationale used *in vivo*, offers a valid approach for investigating the temporal and spatial organization of neuronal ensembles, providing deeper insights into the mechanisms of engram encoding and function. Moreover, the hybrid DLP system enables the precise illumination of individual pre- and post-synaptic sites, allowing for the direct formation of controlled synaptic ensembles. By shaping artificial synaptic ensembles, our system provides a powerful methodology for exploring principles underlying the architectures and configurations of synaptic ensembles. This capability may bridge the gap between AI models and biological research, offering a platform to test and validate theoretical predictions about neural connectivity. As such, it serves as a key resource for advancing our understanding of both natural and artificial neural networks.

After encoding, cell assemblies are subjected to significant changes in the physical and chemical structure of engrams, including reinforced synaptic connections and altered gene expression.[5,26] Our methodology is well suited for investigating these consolidation mechanisms. It allows precise control over stimulation patterns and durations to enhance synaptic plasticity, providing insights into the temporal dynamics of consolidation processing in neural circuits. Additionally, with advanced optical tools for protein manipulation, the system enables exploration of the spatial-temporal aspects of synaptic strengthening, crucial for understanding the dynamics of coordinated circuits and their key synaptic interactions.

Limitations of the study

While the hybrid DLP-based system provides precise optical control of neuronal co-activation, several limitations should be considered. The reduction of complex circuits to two-neuron modules enhances experimental tractability but cannot fully capture the heterogeneity and dynamic interactions present *in vivo*. The artificial induction of synaptic ensembles by patterned illumination may not reflect the full range of physiological activity-dependent processes shaping engrams in the intact brain. Furthermore, the lack of behavioral correlates prevents a direct link between the observed synaptic modifications and memory-related functions. Finally, although the platform enables high spatial and temporal precision, the long-term stability and translational relevance of artificially induced assemblies remain to be established.

RESOURCE AVAILABILITY

Lead contact

Further information and requests for resources and reagents should be directed to and will be fulfilled by the lead contact, Beatrice Vignoli (beatrice.vignoli@cnr.it).

Materials availability

This study did not generate new unique reagents.

Data and code availability

- All data reported in this paper will be shared by the lead contact upon request.
- This paper does not report original code.
- Any additional information required to reanalyze the data reported in this work paper is available from the lead contact upon request.

ACKNOWLEDGMENTS

We thank Antonino Cattaneo for providing -TreP-Arc3′-Nend-PSDTag-Venus-HA-Arc5′UTR and CAG-rtTA-IRES-TdTomato constructs. We thank the MOF facility of the University of Trento. We thank Mattia Mancinelli for his help in

setting up the DLP system and Ca^{2+} imaging analysis. This project has received funding from the European Research Council (ERC) under the European Union's Horizon 2020 research and innovation program, grant number 788793-BACKUP to L.P.; Progetti di Ricerca di Rilevanza Nazionale (PRIN)-Bando 2017, grant number 2017HPTFFCPRIN to M.C.; Fondazione Caritro to C.Z.; and European Union's Horizon 2020 research and innovation program under the Marie Sklodowska-Curie grant agreement no. 101033260 (project ISLAND) to I.A.

AUTHOR CONTRIBUTIONS

M.C., B.V., and L.P. conceived the study; C.Z., A.M., and B.V. performed light-stimulation and Ca^{2+} imaging experiments; A.M. and Y.H. prepared primary cultures; A.M. and B.V. performed immunohistochemistry; C.Z., A.M., and B.V. performed LSC, SD, and SIM acquisitions; C.Z. implemented the DLP setup and the code and performed Ca^{2+} analysis; C.Z. and A.M. performed spine analysis; I.A. and Y.H. performed MEA experiments and analyzed the data; M.C. and B.V. wrote the manuscript with input from C.Z., A.M., and L.P. and in collaboration with all other authors.

DECLARATION OF INTERESTS

The authors declare no competing interests.

DECLARATION OF GENERATIVE AI AND AI-ASSISTED TECHNOLOGIES IN THE WRITING PROCESS

During the preparation of this work, the authors used ChatGPT in order to improve language and readability. After using this tool, the authors reviewed and edited the content as needed and take full responsibility for the content of the publication.

STAR★METHODS

Detailed methods are provided in the online version of this paper and include the following:

- KEY RESOURCES TABLE
- EXPERIMENTAL MODEL AND STUDY PARTICIPANT DETAILS
  - Mice
  - Primary cell culture
- METHOD DETAILS
  - Constructs and viral vectors
  - Experimental plan for DLP light stimulation experiments
  - Immunocytochemistry
  - SD and SIM
  - LSC
  - DLP
  - Calcium imaging
  - Analysis of HA + spines
  - Analysis of cFos+ neurons
  - Live imaging experiments
  - MEA experiments
- QUANTIFICATION AND STATISTICAL ANALYSIS

SUPPLEMENTAL INFORMATION

Supplemental information can be found online at https://doi.org/10.1016/j.crmeth.2025.101265.

Received: October 21, 2024
Revised: June 13, 2025
Accepted: November 18, 2025
Published: January 26, 2026

REFERENCES

1. Josselyn, S.A., and Tonegawa, S. (2020). Memory engrams: Recalling the past and imagining the future. Science *367*, eaaw4325. https://doi.org/10.1126/science.aaw4325.
2. Holtmaat, A., and Caroni, P. (2016). Functional and structural underpinnings of neuronal assembly formation in learning. Nat. Neurosci. *19*, 1553–1562. https://doi.org/10.1038/nn.4418.
3. Poo, M.M., Pignatelli, M., Ryan, T.J., Tonegawa, S., Bonhoeffer, T., Martin, K.C., Rudenko, A., Tsai, L.-H., Tsien, R.W., Fishell, G., et al. (2016). What is memory? The present state of the engram. BMC Biol. *14*, 40. https://doi.org/10.1186/s12915-016-0261-6.
4. Tonegawa, S., Liu, X., Ramirez, S., and Redondo, R. (2015). Memory Engram Cells Have Come of Age. Neuron *87*, 918–931. https://doi.org/10.1016/j.neuron.2015.08.002.
5. Josselyn, S.A., Köhler, S., and Frankland, P.W. (2015). Finding the engram. Nat. Rev. Neurosci. *16*, 521–534. https://doi.org/10.1038/nrn4000.
6. Hebb, D.O. (1949). The organization of behavior (Wiley).
7. Semon, R.W. (1904). Die Mneme als erhaltendes Prinzip im Wechsel des organischen Geschehens (Engelmann) (Biodiversity Heritage Library).
8. Lashley, K.S. (1950). In Search of the Engram (Academic Press).
9. Liu, X., Ramirez, S., Pang, P.T., Puryear, C.B., Govindarajan, A., Deisseroth, K., and Tonegawa, S. (2012). Optogenetic stimulation of a hippocampal engram activates fear memory recall. Nature *484*, 381–385. https://doi.org/10.1038/nature11028.
10. Hayashi-Takagi, A., Yagishita, S., Nakamura, M., Shirai, F., Wu, Y.I., Loshbaugh, A.L., Kuhlman, B., Hahn, K.M., and Kasai, H. (2015). Labelling and optical erasure of synaptic memory traces in the motor cortex. Nature *525*, 333–338. https://doi.org/10.1038/nature15257.
11. Gobbo, F., Marchetti, L., Jacob, A., Pinto, B., Binini, N., Pecoraro Bisogni, F., Alia, C., Luin, S., Caleo, M., Fellin, T., et al. (2017). Activity-dependent expression of Channelrhodopsin at neuronal synapses. Nat. Commun. *8*, 1629. https://doi.org/10.1038/s41467-017-01699-7.
12. Minatohara, K., Akiyoshi, M., and Okuno, H. (2015). Role of Immediate-Early Genes in Synaptic Plasticity and Neuronal Ensembles Underlying the Memory Trace. Front. Mol. Neurosci. *8*, 78. https://doi.org/10.3389/fnmol.2015.00078.
13. Vignoli, B., Sansevero, G., Sasi, M., Rimondini, R., Blum, R., Bonaldo, V., Biasini, E., Santi, S., Berardi, N., Lu, B., and Canossa, M. (2021). Astrocytic microdomains from mouse cortex gain molecular control over long-term information storage and memory retention. Commun. Biol. *4*, 1152. https://doi.org/10.1038/s42003-021-02678-x.
14. Vignoli, B., Battistini, G., Melani, R., Blum, R., Santi, S., Berardi, N., and Canossa, M. (2016). Peri-Synaptic Glia Recycles Brain-Derived Neurotrophic Factor for LTP Stabilization and Memory Retention. Neuron *92*, 873–887. https://doi.org/10.1016/j.neuron.2016.09.031.
15. Vignoli, B., and Canossa, M. (2022). Perirhinal Cortex LTP Does Not Require Astrocyte BDNF-TrkB Signaling. Cells *11*, 1501. https://doi.org/10.3390/cells11091501.
16. Zhang, Y.-P., and Oertner, T.G. (2007). Optical induction of synaptic plasticity using a light-sensitive channel. Nat. Methods *4*, 139–141. https://doi.org/10.1038/nmeth988.
17. Govindarajan, A., Israely, I., Huang, S.-Y., and Tonegawa, S. (2011). The Dendritic Branch Is the Preferred Integrative Unit for Protein Synthesis-Dependent LTP. Neuron *69*, 132–146. https://doi.org/10.1016/j.neuron.2010.12.008.
18. Takahashi, N., Kitamura, K., Matsuo, N., Mayford, M., Kano, M., Matsuki, N., and Ikegaya, Y. (2012). Locally Synchronized Synaptic Inputs. Science *335*, 353–356. https://doi.org/10.1126/science.1210362.
19. Fu, M., Yu, X., Lu, J., and Zuo, Y. (2012). Repetitive motor learning induces coordinated formation of clustered dendritic spines in vivo. Nature *483*, 92–95. https://doi.org/10.1038/nature10844.

20. Cossell, L., Iacaruso, M.F., Muir, D.R., Houlton, R., Sader, E.N., Ko, H., Hofer, S.B., and Mrsic-Flogel, T.D. (2015). Functional organization of excitatory synaptic strength in primary visual cortex. Nature *518*, 399–403. https://doi.org/10.1038/nature14182.

21. Yoshimura, Y., Dantzker, J.L.M., and Callaway, E.M. (2005). Excitatory cortical neurons form fine-scale functional networks. Nature *433*, 868–873. https://doi.org/10.1038/nature03252.

22. Iacaruso, M.F., Gasler, I.T., and Hofer, S.B. (2017). Synaptic organization of visual space in primary visual cortex. Nature *547*, 449–452. https://doi.org/10.1038/nature23019.

23. El-Boustani, S., Ip, J.P.K., Breton-Provencher, V., Knott, G.W., Okuno, H., Bito, H., and Sur, M. (2018). Locally coordinated synaptic plasticity of visual cortex neurons in vivo. Science *360*, 1349–1354. https://doi.org/10.1126/science.aao0862.

24. Han, D.H., Park, P., Choi, D.I., Bliss, T.V.P., and Kaang, B.-K. (2022). The essence of the engram: Cellular or synaptic? Semin. Cell Dev. Biol. *125*, 122–135. https://doi.org/10.1016/j.semcdb.2021.05.033.

25. Guskjolen, A., and Cembrowski, M.S. (2023). Engram neurons: Encoding, consolidation, retrieval, and forgetting of memory. Mol. Psychiatry *28*, 3207–3219. https://doi.org/10.1038/s41380-023-02137-5.

26. Dudai, Y., and Eisenberg, M. (2004). Rites of Passage of the Engram. Neuron *44*, 93–100. https://doi.org/10.1016/j.neuron.2004.09.003.

27. Maccione, A., Gandolfo, M., Massobrio, P., Novellino, A., Martinoia, S., and Chiappalone, M. (2009). A novel algorithm for precise identification of spikes in extracellularly recorded neuronal signals. J. Neurosci. Methods *177*, 241–249. https://doi.org/10.1016/j.jneumeth.2008.09.026.

28. Zhang, X., Yeh, F.-C., Ju, H., Jiang, Y., Quan, G.F.W., and VanDongen, A.M.J. (2020). Familiarity Detection and Memory Consolidation in Cortical Assemblies. eNeuro *7*, ENEURO.0006-19.2020. https://doi.org/10.1523/ENEURO.0006-19.2020.

29. Chiappalone, M., Massobrio, P., and Martinoia, S. (2008). Network plasticity in cortical assemblies. Eur. J. Neurosci. *28*, 221–237. https://doi.org/10.1111/j.1460-9568.2008.06259.x.

STAR★METHODS

KEY RESOURCES TABLE

REAGENT or RESOURCE	SOURCE	IDENTIFIER
Antibodies		
RFP 1:1000	Rockland	Cat. No: 600-401-379; RRID: AB_2209751
HA 1:2000	Abcam	Cat. No: ab9111; RRID:AB_307020
cFos 1:1000	Synaptic Systems	Cat. No: 226008; RRID:AB_2891278
MAP2 1:1000	Covance	Cat. No: SMI-52P; RRID:AB_2728526
SMI 312 1:1000	Covance	Cat. No. SMI-312R; RRID:AB_2314906
PSD95 1:1000	Millipore	Cat. No: #MAB1596; RRID: AB_2092365
GFAP 1:500	Alomone	Cat. No: AGP-307
vGlut1 1:500	Thermo Fisher Scientific	Cat. No: PA5-85764; RRID:AB_2792901
Bacterial and virus strains		
AAV9-hSyn-hChR2(H134R)-EYFP	Addgene	Addgene viral prep # 26973-AAV9; RRID: Addgene_26973
Chemicals, peptides, and recombinant proteins		
TTX	Tocris	Cat. No.:#1069
Doxycicline	Merck	Cat. No.:#D9891
HBSS	Gibco	Cat. No.:#14175053
HEPES	Gibco	Cat. No.:#15630049
PBS	Gibco	Cat.No.:#70011036
Trypsin/EDTA	Gibco	Cat. No.:#25200072
DMEM	Gibco	Cat. No.:#11885084
penicillin-streptomycin 10000 U/ml	Gibco	Cat. No.:#15140163
Poli-L-lysine	Merck Millipore	Cat. No.:#P1399
neurobasal	Gibco	Cat. No.:#21103049
B27	Gibco	Cat. No.:#17504044
Glutamax	Gibco	Cat. No.:#35050061
DAPI	Invitrogen	Cat. No.:#D1306
Aqua Polymount	Polyscience Inc.	Cat. No.:#18606
x-rhod-1 a.m.	Invitrogen	Cat. No.:#X14210
Experimental models: Organisms/strains		
Mice/C57Bl6J	Charles Rivers	N/A
Recombinant DNA		
TreP-Arc3′-Nend-PSDTag-Venus-HA-Arc5′UTR	Prof. A. Cattaneo; Gobbo et al.[11]	N/A
CAG-rtTA-IRES-TdTomato	Prof. A. Cattaneo; Gobbo et al.[11]	N/A
pAAV.CAG.hChR2(H134R)-mCherry.WPRE.SV40	Addgene	Addgene plasmid # 100054; http://n2t.net/addgene:100054; RRID:Addgene_100054);
Software and algorithms		
Nis Element	Nikon	N/A
Prism	GraphPad	N/A
MATLAB	MathWorks	N/A

EXPERIMENTAL MODEL AND STUDY PARTICIPANT DETAILS

Mice

All experiments were conducted in compliance with the Italian Animal Welfare legislation (D.L. 26/2014) that was implemented by the European Committee Council Directive (2010/63 EEC). The procedures were approved by local veterinary authorities and the Italian

Ministry of Health (3FAF3.N.1JY). C57BL/6J mice were used to obtain pregnant dams for embryonic primary cultures. Mice were housed under a 12-h light/dark cycle with food and water *ad libitum*.

Primary cell culture

Cortices were isolated from C57BL/6J mouse embryos (both sex) at embryonic day 17 (E17). In brief, cortical tissues were collected and placed in ice-cold Hank's balanced salt solution (HBSS) with 10 mM HEPES. The tissues were then incubated with 0.25% trypsin-EDTA at 37°C for 20 min. Subsequently, trypsin was carefully aspirated, and the tissues were washed twice with a phosphate-buffered saline (PBS). To neutralize the trypsin, 1 mL Dulbecco's modified Eagle's medium (DMEM), containing 10% fetal bovine serum (FBS) and penicillin-streptomycin (P/S) 10000 U/ml was added. The cortical cells were dissociated using a P1000 pipette, collected by centrifugation (1900 RPM for 5 min), and resuspended in DMEM supplemented with 10% FBS and P/S.

The cells were eventually transfected with 1.5 μg of each DNA construct using the Amaxa Nucleofector system, following the manufacturer's guidelines. After transfection, the cells were plated on glass coverslips pre-coated with poly-L-lysine (0.1 mg/mL). Cells were maintained in a humidified incubator at 37°C with 5% CO_2.

Three hours after plating, the medium was replaced with Neurobasal supplemented with B-27, P/S, and Glutamax. Half of the culture medium was refreshed every 3–4 days. Cells transfected with SA-tdTomato were treated with 1μg/ml of doxycycline for 24 h before light stimulation.

In some experiments, cells were infected at DIV3 with the adeno-associated virus AAV9-hSyn-hChR2(H134R)-EYFP (AAV-ChR2-YFP).

In some experiments, TTX (1μM) was applied 20 min before light stimulation.

METHOD DETAILS

Constructs and viral vectors

The following constructs were used:

-TreP-Arc3′-Nend-PSDTag-Venus-HA-Arc5′UTR[11];

CAG-rtTA-IRES-TdTomato[11];

pAAV.CAG.hChR2(H134R)-mCherry.WPRE.SV40 was a gift from Karl Deisseroth (Addgene plasmid # 100054; http://n2t.net/addgene:100054; RRID:Addgene_100054);

The following viral vector was used.

- AAV9-hSyn-hChR2(H134R)-EYFP was a gift from Karl Deisseroth (Addgene viral prep # 26973-AAV9; http://n2t.net/addgene:26973; RRID: Addgene_26973).

Experimental plan for DLP light stimulation experiments

At DIV11 cortical neurons were placed in a 35 mm dish with a dark bottom, filled with HBSS supplemented with 2 mM $CaCl_2$ and 1 mM $MgCl_2$, for microscopy. Neurons were selected for individual excitations based on the expression of tdTomato (reporting SA) and YFP or mCherry (reporting ChR2). Only neurons with ChR2-YFP/mCherry FI exceeding 200 a.u. were included for stimulation. Preference was given to neurons with at least two processes not oriented in a specific direction.

Light excitations were administered using a pattern of 10 trains of 13 light pulses delivered at 100 Hz, duty cycle 50%, repeated at 0.5 Hz with an intensity of 11 ± 1 mW/mm^2. When two light spots were used, they were spaced 500–1200 μm apart. After light stimulation, coverslips were returned to the incubator with culture media for 90 min, then fixed with cold 4% paraformaldehyde (PFA) for 20 min. Non-illuminated cultures were kept in the dark throughout the entire experimental period.

Immunocytochemistry

Fixed neurons were permeabilized with 0.1% Triton X-100 in PBS for 20 min and blocked with 3% bovine serum albumin (BSA) in PBS for 60 min. Neurons were incubated with primary antibodies diluted in 3% BSA at 4°C overnight. After incubation, the cells were washed several times with 3% BSA and then incubated with fluorophore-conjugated secondary antibodies for 2 h at room temperature. Following this, the cells were washed with PBS, counterstained with DAPI (Invitrogen), and mounted with Aqua Polymount (Polyscience Inc.).

SD and SIM

The microscopy setup, purchased from Crisel Instruments Company, includes the X-Light V2 top-performance confocal spinning disk module and an integrated VCS (Video Confocal Super-resolution) module based on structured illumination microscopy (SIM). The SIM module achieves a lateral resolution of 115 nm and an axial resolution of approximately 250 nm. The system is configured in an upright orientation and incorporates 7 solid-state LED sources with a wavelength range from 395 nm to 640 nm, arranged in the Lumencore Spectra X LED-based light engine. The imaging system is equipped with a Prime Back-Side Illuminated (BSI) Scientific CMOS camera with 2048 × 2048 pixels and a pixel area of 6.5 μm × 6.5 μm. Three objectives are integrated into the system: a dry long-working-distance 10× (LMPLFLN10XLWD, NA 0.25, WD 21mm), a water immersion 60 X (LUMPLFLN60XW, NA 1, WD 2mm),

and an oil 100× (UP objectives UPLSAPO100XO, NA 1.4, WD 0.13 mm). The confocal setup is equipped with spinning disks with double pinhole patterns: one with 40 μm holes and another with 70 μm holes. The 70 μm disk was used for all images in this study.

In SIM mode, the specimen is illuminated with a multipoint beam by filtering the excitation light through a mask and scanning in orthogonal dimensions. Image stacks were acquired with a format of 2048 × 2048 pixels, a z distance of 150 nm, and 36 raw images per plane (multiple acquisition mode x-y grid scan) using a 100× oil objective. The 16-bit depth SIM raw data were computationally reconstructed with the Metamorph software package. Super-resolution algorithms are then employed to compute the final super-resolved image using NIS software.

LSC

LSC was performed using a laser-scanning motorized confocal system (Nikon A1) equipped with an Eclipse Ti-E inverted microscope and four laser lines (405, 488, 561 and 638 nm). z series images were taken with an inter-stack interval of 0.3 or 0.5 μm using a 60X oil immersion objective (Nikon APO 60× 1.4).

DLP

A DLP E4500 purchased from E.K.B Technologies Ltd. equipped with 3 LEDs, optics, a WXGA DMD (Wide Extended Graphics Array Digital Micromirror Device), and a driver board was integrated into the EPI-fluorescence port of SD microscope. The DLP's light engine can generate approximately 150 lumens at 15 W of LED power consumption. Specifically, a blue LED with a wavelength of 460 ± 14 nm and a power output of 600 mW was utilized. The DMD features 1039680 mirrors arranged in a diamond array configuration of 912 columns by 1140 rows, enabling patterned illumination using preloaded and custom patterns. The system supports temporal pulsing of light with internal and external triggers, with a minimum exposure time ranging from 235 μs to 8333 μs, depending on the bit depth of the projected image. It handles 1 to 8-bit images at a resolution of 912 columns × 1140 rows, ensuring pixel accuracy where each pixel corresponds to a micromirror on the DMD. The emitted light from the DLP system is aligned with the microscope's optical path via the system's rear port using a zoom lens and a tube lens. A dichroic mirror (Chroma T505lpxr-UF1) serves as a high-pass filter, reflecting wavelengths smaller than 505 nm. This setup enables simultaneous DLP illumination and signal recording at longer wavelengths.

To determine the light power reaching the specimen, we employed a power meter beneath the microscope objective (Ophir Nova, PD300).

Light delivery

The DLP achieves varying levels of resolution, defined as the full-width half maximum (FWHM) of the illuminated region on the sample plane when a single pixel of the DLP matrix is activated. Specifically, with a 10× air objective, the resolution is 5.4 ± 0.2 μm when the aperture stop (AS) is fully closed to minimize optical aberrations (Figure S1C). With the AS open, the resolution is slightly reduced to 8 ± 5 μm. Using a 60× water immersion objective, significantly improves the resolution, reaching 0.90 ± 0.07 μm with the AS closed (Figure S1C) and 1.1 ± 0.6 μm with the AS open.

The light distribution on the sample plane was initially not uniform (Figure S1A), causing variations in light intensity experienced by neurons at different positions within the FOV. To correct this issue, we rectified the non-uniform light distribution mapping the wide-field light intensity distribution on the sample plane and we used it as a reference for normalizing the desired black-and-white light pattern. This pattern was then loaded into the DLP software as an 8-bit image. Additionally, we verified that configuring the DLP with a high bit depth did not affect the temporal patterns used in our experiments. This approach allowed us to enhance the uniformity of the light distribution, especially at the center of the FOV (Figure S1A).

To determine the light power reaching the specimen, we employed a power meter beneath the microscope objective (Ophir Nova, PD300), and the intensity at the sample plane was calculated by adjusting for the illumination area.

We ensured a consistent average intensity of 11 ± 1 mW/mm^2 across the entire FOV. Careful adjustment of the aperture (AS) and field stop (FS) positions confined the illumination to the desired FOV, improving the correction of optical aberrations and contrast.

Pattern characterization

To achieve single-cell excitation within the neuronal network, we designed localized light spots at specific positions for each experiment. These spots were set to have diameters ranging from 10 to 40 μm (Figure S1B). Since the average distance between ChR2-expressing neurons in our cultures is approximately 170 μm, the dimensions of a single spot, centered on a cell body, are optimal for precise single-cell excitation. Regarding contrast, defined as (max-min)/min*100, the average contrast of the single spot across the FOV was (5 ± 2) x 10^4 relative to the background signal. However, when multiple spots were projected simultaneously (24 spots; Figure S1D), the background signal increased, resulting in a contrast value of (16 ± 5) x 10^3.

Two-spots illumination

Most of our study focused on two-spot illumination using a 10× objective. To determine the minimum distance at which two spots are considered separated, we projected pairs of spots at different distances and analyzed their intensity profiles. Specifically, we evaluated the ratio between the valley intensity and the average of the two peak intensities (valley/peak). We accounted for potential aberrations that could affect the minimum distance between spots differently in the vertical (Figure S1E) and horizontal (Figure S1F) directions. To address this, we averaged the valley/peak values in both the vertical and horizontal directions, finding that the separation reached the value of 0 at approximately 120 μm (Figure S1G).

Light stimulation of dendritic spines

The illuminated area had a diameter of 45 ± 8 μm and was positioned 18 ± 4 μm away from the cell body.

Light to noise characterization

To eliminate potential interference or noise from multiple reflections between the glass coverslip, where neurons are plated, and the Petri dish containing the buffer solution, we performed all characterizations on a reflective surface placed at the sample plane and immersed in distilled water.

Although cell bodies can influence light transmission, and the coverslip can cause multiple reflections between the glass and the dish's plastic, we considered this noise negligible compared to the direct light emitted by the DLP. Nonetheless, to further minimize reflections at the dish-air interface during experiments, we used dishes with black bottoms. This approach helped to reduce potential light noise, ensuring the accuracy of our observations.

Calcium imaging

At 10–13 DIV cells were treated with X-Rhod-1 AM (1μM) in HBSS supplemented with $CaCl_2$ (2mM) and $MgCl_2$ (1mM) at 37°C for 30 min. Subsequently, the cells were washed with supplemented HBSS at 37°C. After 30 min, coverslips were positioned under the spinning disk microscope in a 35 mm dark bottom dish with supplemented HBSS.

The FI of X-Rhod-1 was monitored by acquiring time-lapses at 1.5 Hz for about 3 min. At frame 100 of the timelapse, LTP light stimulation (10 trains of 13 light pulses delivered at 100 Hz, duty cycle 50%, repeated at 0.5 Hz) from the DLP was applied. During DLP stimulation, the camera was triggered to acquire only during intervals when the DLP light was off (i.e., between the 10 light trains). The resulting timelapse file was then analyzed using a custom MATLAB program designed to identify neuronal bodies (ROIs) and extract calcium traces based on X-Rhod-1 fluorescence in these ROIs over time.

Automated detection. For region of interest (ROI) identification, the process begins with creating an average image from all frames captured before excitation. This average image is divided into 50 intensity levels, used as minimum thresholds for generating binary images. To isolate neuronal cell bodies, the regionprops function in MATLAB is used to extract essential information from the analyzed regions. This information encompasses parameters such as area, centroid coordinates, axis dimensions, and intensity values; the process is performed on all the binary images and ROIs duplicates are then removed by evaluating the distances between their centroids.

Ca^{2+} signal normalization. To process the multi-tiff images, we perform the following steps for each frame.

1. Calculate the average pixel intensity within identified ROIs to create temporal traces of calcium fluorescence.
2. To eliminate baseline fluorescence noise, we normalize the entire trace using a linear fit that extends up to the excitation point. This helps in setting a consistent baseline for comparison.
3. To distinguish calcium response traces from the noise, we use specific parameters:

ΔF/F: represents the ratio of the difference (ΔF) between the maximum fluorescence level during light stimulation and the baseline fluorescence level (F), which is the average of all frames before stimulation, to F.

Σ: indicates the maximum absolute variation of the fluorescence trace before the onset of light stimulus.

4. To classify traces as responses, we apply threshold values to these parameters. Specifically, we require: (i) ΔF/F to be greater than 0.03, indicating a significant increase in fluorescence during stimulation; (ii) $\frac{\Delta F}{F}/\Sigma$ to be greater than 1.2, ensuring that the increase in fluorescence is significantly higher than any potential pre-stimulation fluctuations.

We classified a trace as a response when calcium indicator fluorescence changed above thresholds at the stimulation time. We calculated ΔF/F to quantify the change in fluorescence in these responsive neurons.

Analysis of HA + spines

Imaging processing was conducted using the NIS Elements software from Nikon. Confocal images underwent cropping, focusing on segments of dendrites proximal to the cell body within 30–60 μm range. Subsequently, spines along the dendritic processes were morphologically identified using the tdTomato cellular filler. Manual quantification of spines expressing the HA signal (HA+) was performed on single stack images, and the results were expressed as a percentage relative to the total number of spines for each cropped dendrite. Cells subjected to light stimulation were categorized as "illuminated" neurons while neighboring non-illuminated neurons within the field of view were designated as "non-illuminated" cells. Cells located far from the stimulated area were classified as "out-FOV". The percentage of HA + spines was normalized over the outFOV values.

To investigate the distribution of HA + spines within the network, polar plots were generated to map the orientation of dendritic processes in stimulated cells and their corresponding percentage of HA + spines. Specifically, for each stimulated cell, angles were measured between the imaginary line connecting the centers of cell bodies (defined as 0°) and the direction of the proximal part of the dendrites. Subsequently, polar plots were created associating each dendrite's direction (angle) with its percentage of HA + spines. The data were then categorized into "IN" and "OUT" processes based on their location in the first/fourth quadrant (facing the second neuron) of the polar plot or the second/third quadrant, respectively. For comparative analysis, for each cell the percentage of HA + spines for all dendrites was normalized on the average of "OUT" processes.

Analysis of cFos+ neurons

To define a neuron as c-Fos positive we established a threshold for each experiment based on the averaged c-Fos fluorescence intensity of non outFOV -stimulated neurons, minus the standard error of the mean (SEM). The percentage of c-Fos positive neurons was calculated using the formula: (Number of c-Fos positive neurons)/(Total number of neurons) $\times$100.

Live imaging experiments

Live imaging experiments were performed at DIV 13 on cultures transfected with SA and ChR2-mCherry. Coverslips were placed in a dark bottom 35 mm dish containing HBSS, $CaCl_2$ (2mM) and $MgCl_2$ (1mM). The dish was placed in the Okolab stage incubator system (H301-UP), equipped with H301-T-UNIT-BL-PLUS electric top stage incubation system, maintaining a constant temperature of 37°C. Cells expressing tdTomato/mCherry with clearly defined dendrites and visible spines were selected for observation. Two neurons were selected for spot LTP-like illumination using the DLP and a 10$\times$ objective with an 11 $\pm$ 1 mW/mm^2 intensity. The expression of Venus and tdTomato/mCherry was monitored using the 60$\times$ water immersion objective, acquiring confocal images before, 60 min and 90 min after stimulation. Images were acquired by averaging 4 images for each z-stacks at 0.5 μm step size.

MEA experiments

A MEA-2100mini system from Multichannel Systems GmbH (MCS) was used to record the electrical activity of neuronal cultures. The cultures were plated on electrode array chips (60MEA-200/30iR-Ti-gr by MCS) featuring 60 titanium-nitride electrodes embedded in glass and enclosed by a glass ring. The electrodes have a diameter of 30 μm and a pitch of 200 μm. The chips are placed on a headstage device that samples the culture's electrical signals. The collected signals are amplified and filtered by a signal collecting unit (SCU), then digitalized and read by software.

In our experimental procedure, the DLP system delivered optical stimulation within a circular area with a diameter of approximately 200 μm. Initially, neurons were exposed to a baseline illumination pattern, featuring 20 ms light pulses at a frequency of 0.5 Hz for 10 min. Then, to induce LTP, neurons underwent a stimulation regimen that included 10 sets of 13 light pulses delivered at 100 Hz, with a repetition frequency of 0.5 Hz. After the LTP stimulus, neurons were subjected to baseline illumination patterns at four different time points: 0, 20, 40, and 60 min post-stimulation.

The recording is performed using MCS experimenter software, where the signals can be digitally filtered, inceptively analyzed, and tracked in real-time. The signals were sampled at 20KHz. The recorded files are saved and exported for subsequent offline analysis to identify neuronal spikes. Initially, raw signals underwent digital filtering with a band-pass Butterworth filter with cutoff frequencies set at 0.3 and 3 KHz. Spikes were detected using a Precise Timing Spike Detection (PSTD) algorithm.[27] To analyze the responses of the neuronal network to light stimulation, we used post-stimulus time histograms (PSTHs) at each electrode, counting the number of spikes within predefined time bins of fixed width and distance relative to the light pulse, averaged over the number of pulses. Electrodes were excluded from the analysis if they exhibited very low activity or unstable behavior, based on two criteria: an activity threshold and a stability threshold. The activity threshold was defined as an area under the PSTH curve of less than '1' during the baseline step.

Stable electrodes were identified by calculating the absolute change $|\Delta P|/P$ (where P is the PSTH area of the reference baseline) across two consecutive recordings without LTP stimulation; electrodes with variations greater than 20% were excluded. The remaining electrodes were used to assess efficacy. For these electrodes, the baseline PSTH area relative change ($\Delta P/P$) was calculated between two recordings prior to LTP-pattern exposure (Figure 1 D, -10-0 min). After LTP stimulation, efficacy was calculated as the $\Delta P/P$ between pre- and post-stimulation phases, considering only electrodes with a positive $\Delta P/P$[28] (Figure 1D, 0-10, 20-30, 40-50, and 60-70 min).

The Potentiation Index (PI) was subsequently determined as the percentage of electrodes exceeding a 20% efficacy threshold at each time point among the selected channels, offering valuable insights into the temporal progression of potentiation.[29] PI values greater than 0 indicate the presence of potentiation within the network, underscoring the extent of network-wide engagement over time.

QUANTIFICATION AND STATISTICAL ANALYSIS

All statistical analysis were performed using GraphPad Prism version 10.0.0, GraphPad Software, Boston, Massachusetts USA, www.graphpad.com PRISM. All violin plots depict median (continuous line) and quartiles (dashed line). All data were run for the Shapiro-Wilk normality test. Statistical comparisons were performed using a *t* test or one-way ANOVA test for normally distributed data and Mann-Whitney or Kruskal-Wallis tests for non-normally distributed data. Details on the sample number n, the type of statistical test used, and the significance of the data are provided in the figure legends. A p-value <0.05 was considered statistically significant.